Ampsa

Design Smarter Amplifiers

Ampsa Amplifier Design Wizard

Powered by Clipping Theory and Differential Evolution

Pieter Abrie
Ampsa (Pty) Ltd.

11/25/2025

Innovative Amplifier Design Tools

Second-Harmonic Input Distortion

When the input power increases, the nonlinear input capacitor in a FET or HEMT or bipolar transistor generates harmonic components that can degrade the performance of an amplifier stage designed without considering the effect of this nonlinearity on the output circuit. Second-harmonic input distortion was explored in detail in [1]. If the ratios of the second-harmonic and fundamental components of the intrinsic input voltages ($H2DR = V_{1i\_H2} / V_{1i\_Fu}$) are known and these voltages are out of phase, the optimum intrinsic load terminations were calculated for specific classes of operation. The optimum load terminations associated with arbitrary phase differences were presented in [2, 3].

It was also shown that when the relative phase of the intrinsic second-harmonic input voltage lies within either [270°; 360°] and [0°; 90°], the efficiency becomes higher than in the ideal case with no second-harmonic input content. (Inside these ranges, the conduction angle of the intrinsic output current is less than 180°.) However, he output power will be lower. The performance of inverse Class-F stages was also found to be resistant to any second-harmonic input voltage when the relative phase lies within [90°; 270°]. Due to the reduced conduction angles, the efficiency of inverse Class-F stages nonetheless improves outside this range.

References [1] - [3] provide insight into the impact of the input nonlinearity on the output circuit and demonstrate the potential for improving efficiency. The challenges are knowing the *H2DR* ratio in advance and recognizing that the region with very high efficiency is narrow and close to the regions of poor efficiency.

The second-harmonic source impedance presented to an amplifier stage can be manipulated to reduce any degradation in performance. The standard approach is to map power and efficiency contours to the second-harmonic source impedance presented at the input of the transistor with the load network in-place. The input network is then designed to match the fundamental impedances, to stabilize the transistor (with gain levelling, if possible) and to optimize the power and the efficiency. With the input network in place, the complete circuit can be tuned or optimized.

Extrinsic second-harmonic shorts with minimal loading at the fundamental frequencies are often used to improve the performance of an amplifier stage. For relatively narrow passbands, this approach works well. In wideband designs, a different strategy may be required, although extrinsic harmonic shorts can still enhance performance over portions of the passband.

Source-pull contours show that the power and efficiency at each passband frequency are generally acceptable over large areas of the Smith chart, while poor or very good performance occurs only in small regions. Because the region with very good performance lies very close to the region of poor performance, it may be more practical to avoid both extremes. Given the many demands on the input network, this approach is often more realistic.

To minimize *H2DR*, an intrinsic second-harmonic short is required (that is, if possible). The intrinsic source impedance presented to the nonlinear capacitor in the input circuit is, therefore, of interest.

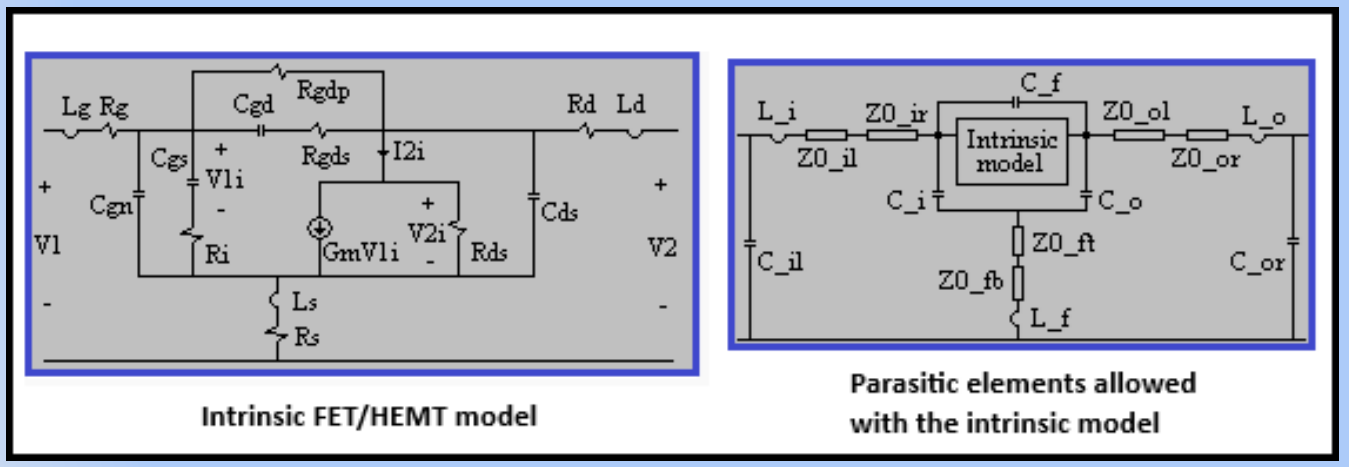

Figure 1. The model used for FET or HEMT transistors in the ADW. The intrinsic model can be extended with the parasitic elements shown.

The equivalent circuit used in the ADW for FET or HEMT transistors is shown in Figure 1. Note that voltage-shunt and current-series feedback are provided for in the equivalent circuit. To calculate the second-harmonic Thevenin impedance (Z_{Si_H2}) associated with C_{gs} by using nodal analysis, the capacitor must be replaced with a current source, all the ground connections in the circuit must be floated (new node number) and the bottom node of the new current source must be defined as ground. Alternatively, the capacitor can be replaced with two grounded current sources with $I_{cs1} = -I_{cs2}$. In the ADW, the intrinsic source impedances are calculated by using power parameters. The calculated second-harmonic impedances are listed in a table, with the input VSWRs and the output power for the stage of interest.

The intrinsic second-harmonic voltage is determined by the intrinsic second-harmonic current generated by the time domain voltage across the nonlinear input capacitor and the $C(V)$ profile of this capacitor ($I_{1i}(t) = C_{gs}(V_{1i}) \times dV_{1i}(t)/dt$). The harmonic components of $V_{1i}(t)$ are determined by the harmonic current components and the Thevenin impedances presented to the capacitor by the complete circuit at each harmonic. With the load network not designed yet, the Thevenin impedances are not known and *H2DR* cannot be calculated. The exception is of course when the transistor is unilateral ($s_{12} = 0$).

To serve as a design aid, *H2DR* is approximated in the ADW by using the following equation:

$$H2DR = V_{1i\_H2} / V_{1i\_Fu} = (- I_{1i\_H2} \times Z_{Si\_H2}) / (I_{1i\_Fu} / (j\omega_{Fu} \times C_{gs}))$$

$$= - [\alpha_{V1i} \, \mathrm{EXP}(- j \, \beta_{V1i})] \times Z_{Si\_H2} \times j\omega_{Fu} \times C_{gs} \qquad \text{(Equation 1)}$$

with

$$I_{1i\_H2} = - [\alpha_{V1i} \, \mathrm{EXP}(- j \, \beta_{V1i})] \times I_{1i\_Fu} \qquad \text{(Equation 2)}$$

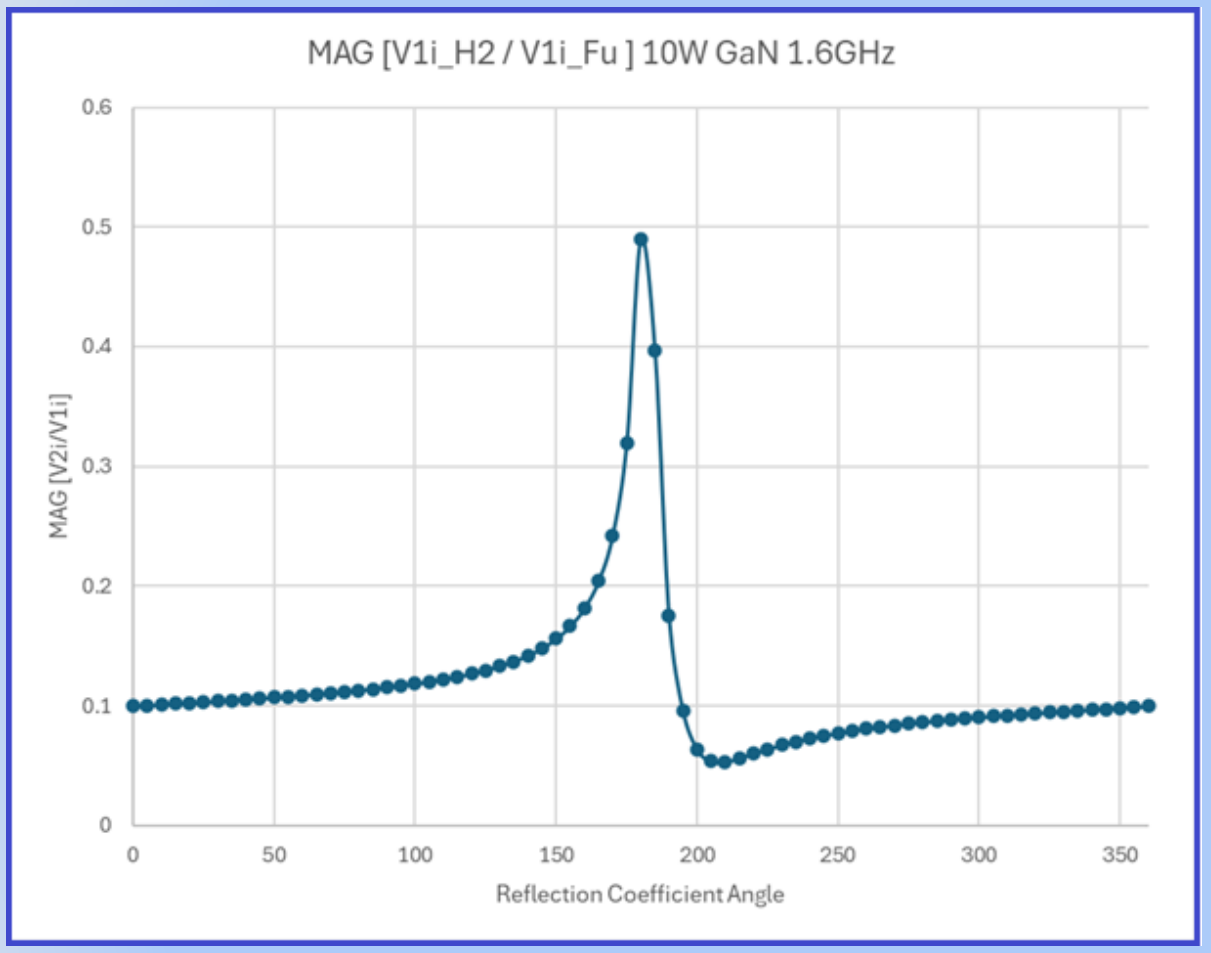

Figure 2. The magnitude of the V_{1i_H2} to V_{1i_Fu} ratio (10W GaN transistor) as a function of the source-pull reflection coefficient angle.

Note the assumption in (1) that the fundamental-frequency impedance is not changed significantly by the nonlinearity.

A harmonic-balance simulation with access to the intrinsic input circuit is required to calculate α_{V1i} and β_{V1i}. V_{1i_H2} /V_{1i_Fu} can then also be calculated directly.

The magnitude of V_{1i_H2}/V_{1i_Fu} was calculated for a 10W GaN transistor as a function of the source-pull reflection coefficient at the gate terminal by using harmonic balance and is shown in Figure 2. Note the resonance behavior and the range of the magnitude values (maximum 0.49, minimum around 0.05).

In the ADW, α_{V1i} is taken to be one, and the fundamental-frequency and the second harmonic intrinsic currents in the nonlinear capacitor are assumed to be in-phase when *H2DR* is calculated.

ADWDsgn4.ani - Second-Harmonic Input Distortion Factors and Intrinsic Source Impedances

FREQ_Fu (GHz)	RSi_H2 (Ohm)	XSi_H2 (Ohm)	QSi_H2 (-)	H2DR_MAG (-)	H2DR_ANG (Deg)	VSWRi (-)	Power (dBm)
1.00	5.60	-7.27	-1.30	0.4670	217.60	5.40	41.13
1.10	5.24	-6.39	-1.22	0.4629	219.38	4.26	41.51
1.20	5.17	-5.60	-1.08	0.4654	222.71	3.41	41.79
1.30	5.26	-5.00	-0.95	0.4803	226.48	2.78	42.01
1.40	5.41	-4.63	-0.85	0.5075	229.49	2.32	42.13
1.50	5.48	-4.45	-0.81	0.5392	230.94	2.02	42.16
1.60	5.36	-4.32	-0.81	0.5610	231.13	1.86	42.12
1.70	5.12	-4.02	-0.78	0.5632	231.89	1.84	42.00
1.80	5.05	-3.45	-0.68	0.5607	235.62	1.93	41.79
1.90	5.46	-2.91	-0.53	0.5980	241.97	2.11	41.58
2.00	6.21	-3.03	-0.49	0.7034	243.96	2.35	41.42
2.10	6.19	-3.77	-0.61	0.7746	238.63	2.62	41.37
2.20	5.63	-3.90	-0.69	0.7667	235.30	2.92	41.40
2.30	5.35	-3.67	-0.69	0.7597	235.54	3.23	41.48
2.40	5.29	-3.50	-0.66	0.7755	236.54	3.54	41.61
2.50	5.29	-3.47	-0.66	0.8058	236.72	3.84	41.71
2.60	5.21	-3.58	-0.69	0.8369	235.54	4.13	41.76
2.70	4.96	-3.72	-0.75	0.8525	233.13	4.40	41.79
2.80	4.52	-3.75	-0.83	0.8374	230.27	4.66	41.82
2.90	4.00	-3.53	-0.88	0.7874	228.55	4.90	41.80
3.00	3.63	-3.03	-0.84	0.7230	230.14	5.11	41.78
3.10	3.56	-2.52	-0.71	0.6883	234.67	5.28	41.77
3.20	3.61	-2.10	-0.58	0.6798	239.83	5.38	41.79
3.30	3.76	-1.75	-0.47	0.6972	245.00	5.36	41.85
3.40	3.99	-1.53	-0.38	0.7394	248.99	5.19	41.87
3.50	4.25	-1.47	-0.35	0.8019	250.91	4.85	41.86
3.60	4.48	-1.70	-0.38	0.8781	249.23	4.37	41.79
3.70	4.10	-2.38	-0.58	0.8936	239.91	3.81	41.60
3.80	2.76	-1.66	-0.60	0.6233	238.93	3.35	41.21

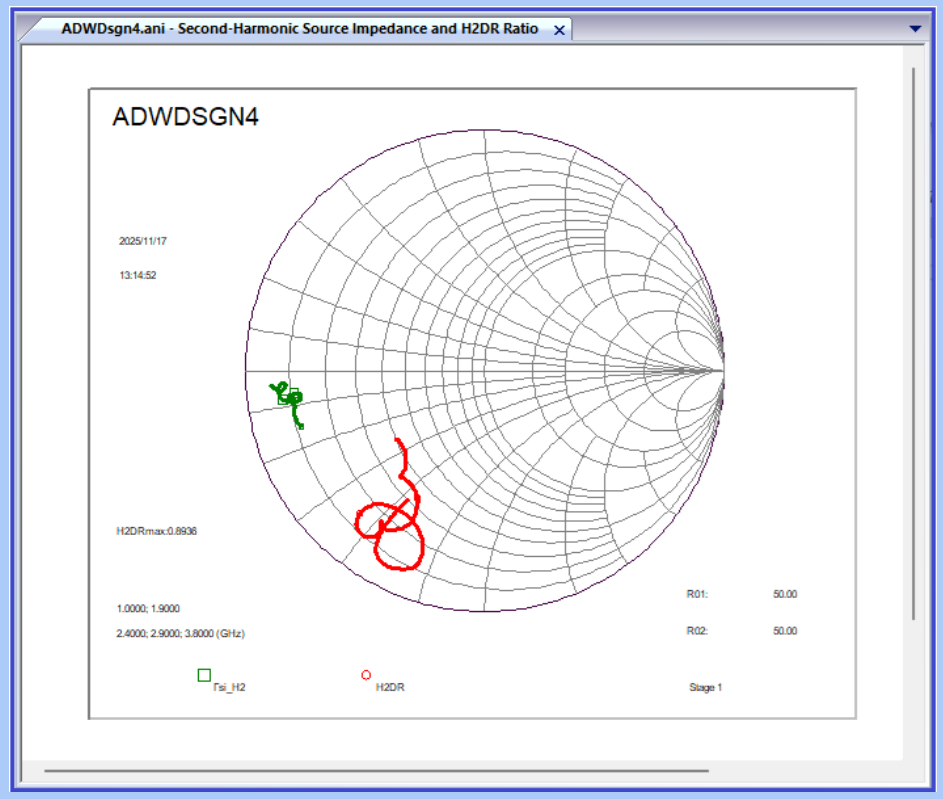

Figure 3. The information displayed in an ADW second-harmonic input distortion table and graph.

Examples of the table and graph created in the ADW for the second harmonic intrinsic source impedance (Z_{si_H2}) and the *H2DR* magnitude and phase over the passband of interest are provided in Figure 3.

Note that in this example the magnitude of Z_{si_H2} decreases with increasing frequency. The *H2DR* phase is in the range [217°, 251°].

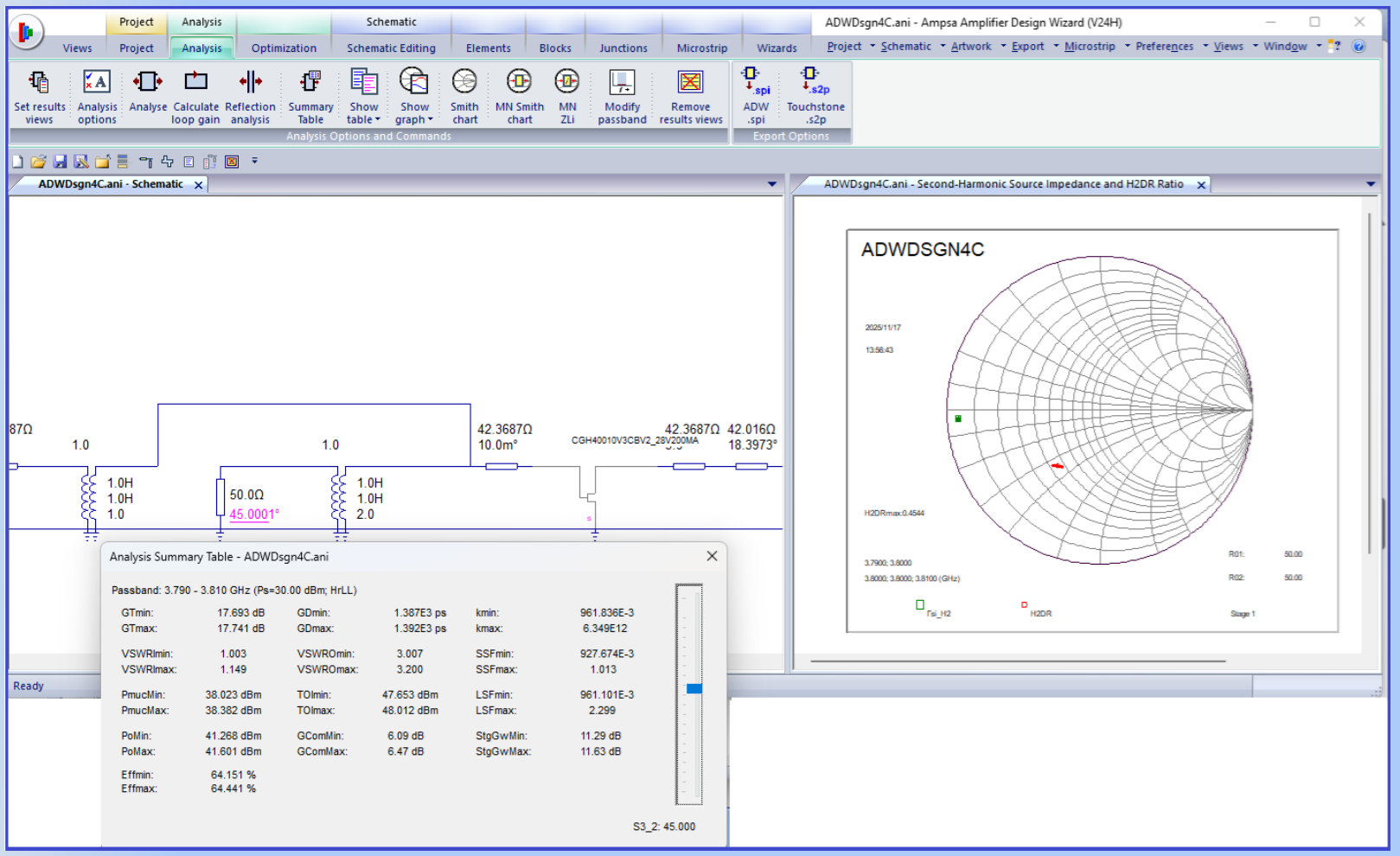

Figure 4. An example of an ADW source-pull circuit.

A source-pull circuit can be set up in the ADW to calculate the *H2DR* and the C_{gs} Thevenin impedance as a function of the length of a shorted or open-ended stub. Such a circuit is shown in Figure 4. The transformer on the left is active in the passband and presents open outside the passband. The transformer on its right performs the same function for the second harmonics. The passband and the harmonic bands must not overlap.

The circuit can be analysed with different lengths for the shorted stub and data obtained can be plotted in a third-party application. The option to record the tuning traces is also provided (see Figure 5). The data associated with the memory traces can be listed in the ADW. The listed information can be exported and plotted externally. Note the option to clear any memory traces associated with a graph.

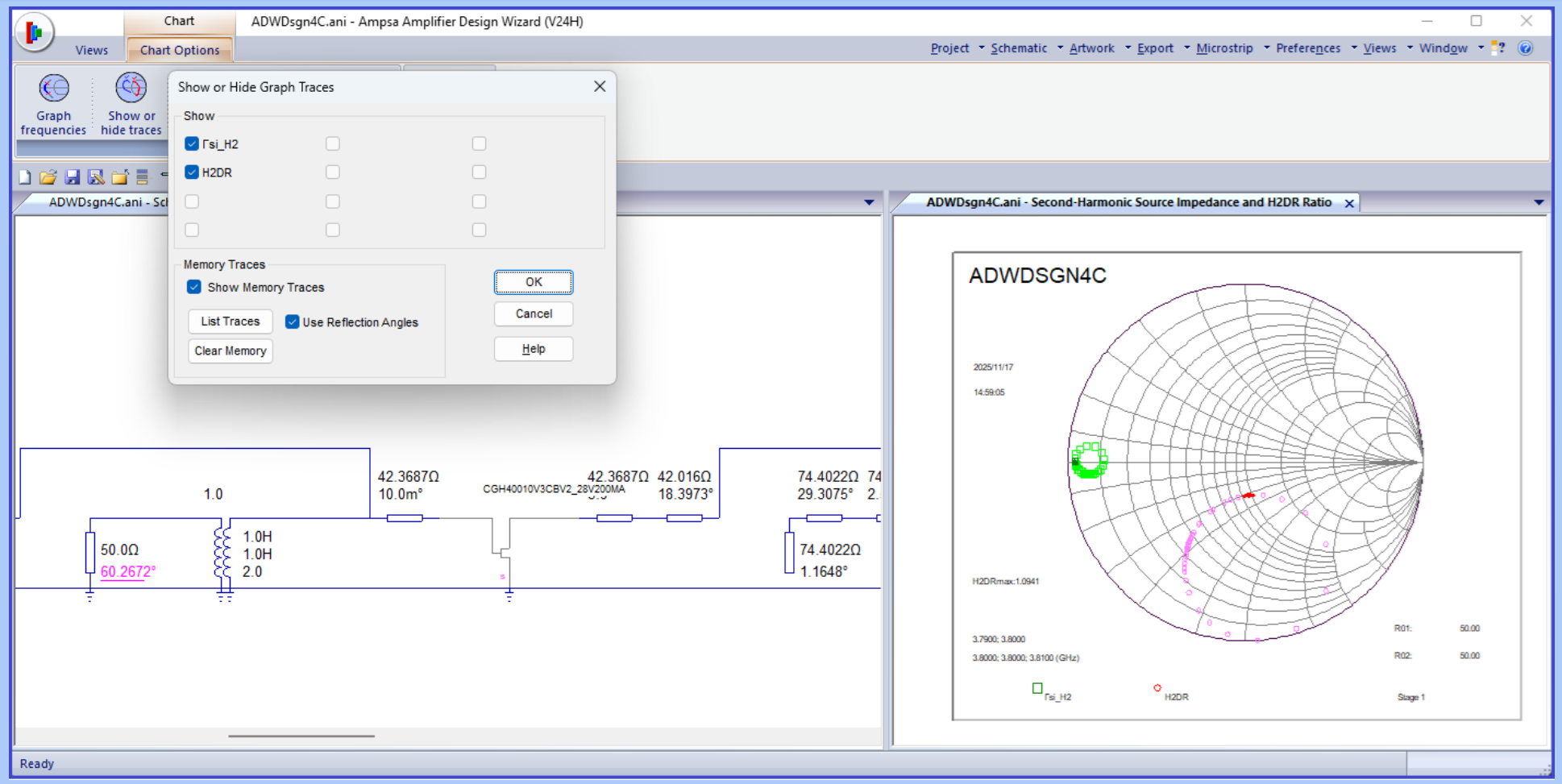

Figure 5. The Chart Option menu for a graph can be used to create memory traces when a schematic variable is tuned in the ADW.

ADWDsgn4C.ani - Tuned Second-Harmonic Input Distortion Factors and Intrinsi...

REFL_ANG (Deg)	RSi_H2 (Ohm)	XSi_H2 (Ohm)	QSi_H2 (-)	H2DR_MAG (-)	H2DR_ANG (Deg)
9.21	1.93	-1.47	-0.76	0.4698	232.81
13.33	1.96	-1.49	-0.76	0.4764	232.82
29.82	2.06	-1.55	-0.76	0.4989	232.92
33.95	2.08	-1.57	-0.75	0.5038	232.96
79.31	2.28	-1.68	-0.74	0.5483	233.53
101.15	2.37	-1.73	-0.73	0.5668	233.88
128.80	2.48	-1.78	-0.72	0.5905	234.41
150.64	2.59	-1.81	-0.70	0.6113	234.94
153.54	2.60	-1.82	-0.70	0.6143	235.03
212.50	3.11	-1.93	-0.62	0.7078	238.20
220.75	3.25	-1.94	-0.60	0.7316	239.19
233.12	3.54	-1.93	-0.55	0.7795	241.39
237.24	3.67	-1.91	-0.52	0.8003	242.44
241.37	3.82	-1.89	-0.49	0.8245	243.73
249.61	4.23	-1.76	-0.42	0.8860	247.43
253.74	4.50	-1.62	-0.36	0.9252	250.17
257.86	4.82	-1.39	-0.29	0.9709	253.86
261.99	5.18	-1.01	-0.19	1.0218	258.98
266.11	5.52	-0.37	-0.07	1.0705	266.20
270.23	5.63	0.62	0.11	1.0955	276.29
274.36	5.14	1.81	0.35	1.0539	289.45
278.48	3.90	2.61	0.67	0.9079	303.80
282.60	2.51	2.53	1.01	0.6895	315.23
286.73	1.59	1.89	1.19	0.4779	319.90
290.85	1.17	1.18	1.01	0.3207	315.24
294.98	1.03	0.59	0.57	0.2300	299.71
299.10	1.03	0.14	0.14	0.2019	277.96
303.22	1.09	-0.19	-0.17	0.2141	260.26
307.35	1.17	-0.44	-0.37	0.2413	249.49
315.60	1.33	-0.78	-0.59	0.2980	239.63
319.72	1.40	-0.90	-0.64	0.3223	237.35
327.97	1.53	-1.08	-0.70	0.3623	234.91
332.09	1.59	-1.14	-0.72	0.3788	234.24
336.21	1.64	-1.20	-0.73	0.3934	233.78
348.59	1.77	-1.33	-0.75	0.4288	233.07
352.71	1.81	-1.37	-0.75	0.4384	232.96

Table 1. An example of a memory trace table.

An example of a table created with ADW memory trace data is shown in Table 1. Instead of listing the data as a function of stub length, the option to list the data as a function of the reflection coefficient angles was used here (see the option in Figure 5).

Note: The intrinsic *Q*-values are positive when the *H2DR* phase is in the range [270°; 360°] or [0°; 90°].

The magnitudes and phases of *H2DR* and the *Q*-values for the intrinsic source impedance (Z_{Si_H2}) listed in Table 1 are plotted in Figure 6 versus the reflection coefficient angles.

Note that the *H2DR* phase is almost constant (around 232° at 3.8GHz) at most of the reflection coefficient angles but changes sharply over the Q_{Si} resonance range. This is also the reason why the markers in Figure 5 are sparsely distributed for tuning angles away for the constant phase region.

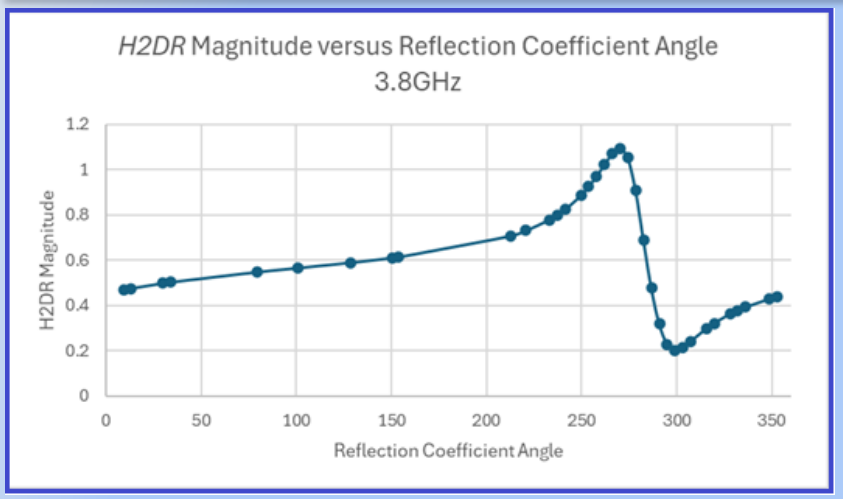

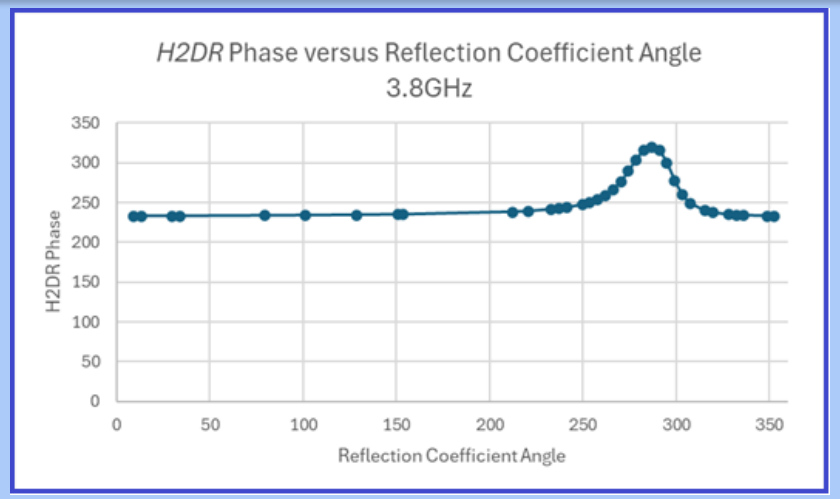

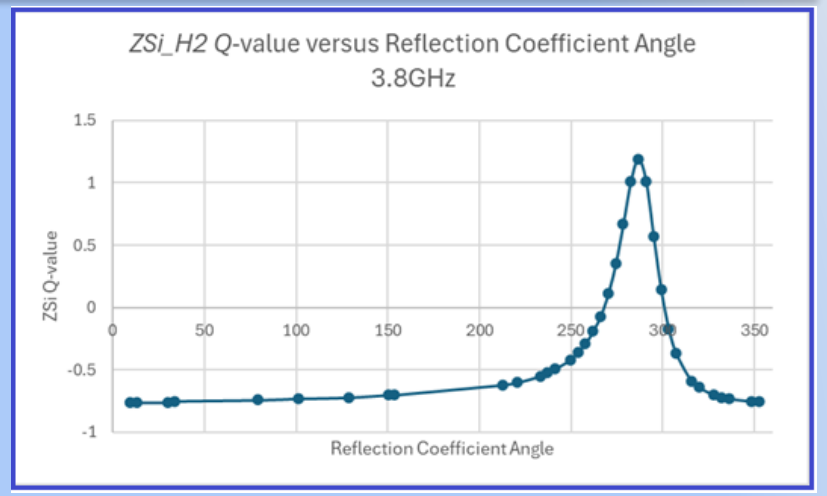

Figure 6. The *H2DR* magnitude and phase and the *Q*-value associated with Z_{Si} are plotted versus the source-pull reflection coefficient angle.

The *H2DR* magnitude and phase are plotted for the amplifier stage in Figure 5 (Macom 10W GaN transistor) at three passband frequencies (1.4 GHz, 2.6 GHz and 3.8 GHz) in Figure 7. The regions over which the *H2DR* phase changes significantly are marked in these plots.

Note that the *H2DR* phases in Figure 7 are almost constant for most of the tuning range at all the frequencies considered. Approximate values for the phase angles in the constant regions are shown below:

1.4 GHz: 193° 2.6 GHz: 225° 3.8 GHz: 233°.

Harmonic-balance source-pull graphs at the same frequencies were created for this amplifier stage in Microwave Office™ and are shown in Figure 8. Note that while there is an upward shift with increasing frequency, the correlation between the *H2DR* phase and the power and efficiency graphs is very good. Also note the proximity of the reflection coefficients for the best and the worst efficiency.

The power is low when the efficiency is maximum in the source-pull graphs.

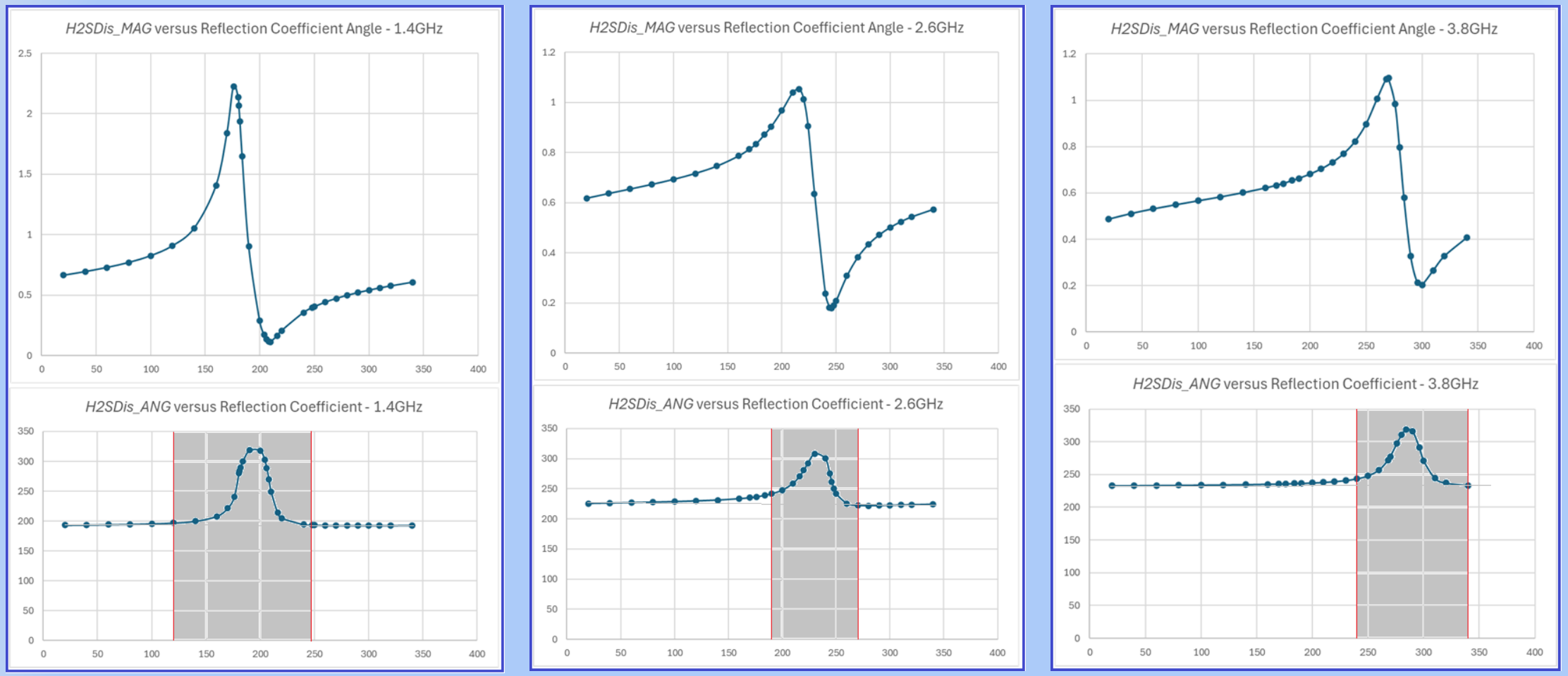

Figure 7. The ADW *H2DR* magnitude and phase for an amplifier stage at three different passband frequencies.

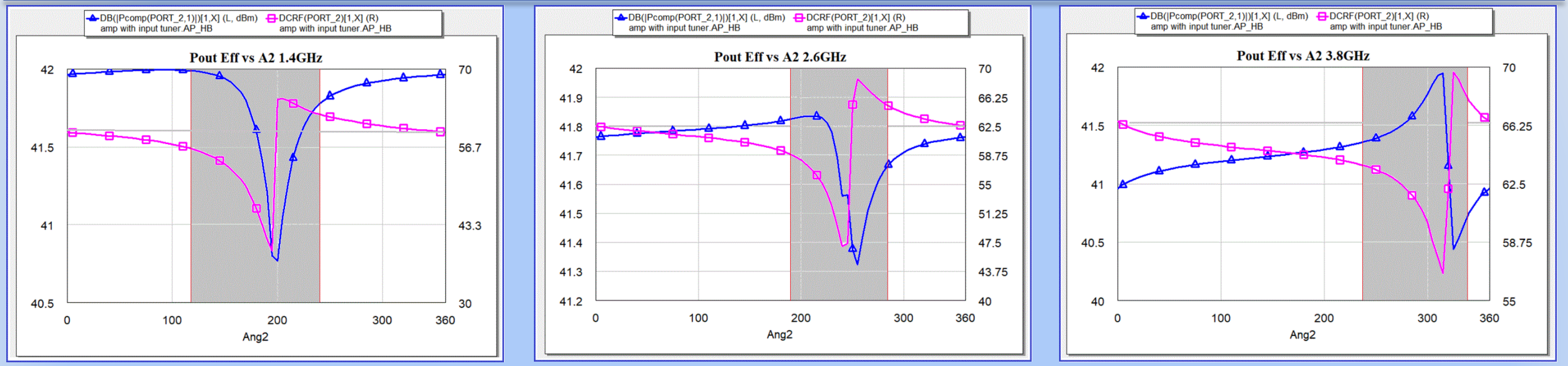

Figure 8. The power and efficiency for the amplifier stage of Figure 6 as calculated in Microwave Office™.

It follows from the graphs in Figure 8 that for peak efficiency, the values for the second-harmonic reflection coefficient angles must be as shown below. Note that the angles associated with the worst efficiency are very close to these angles (2.8 GHz: 198°; 5.2 GHz: 245°; 3.8 GHz: 312°).

2.8 GHz: $\theta_R = 200°$ 5.2 GHz: $\theta_R = 253°$ 7.6 GHz: $\theta_R = 325°$

The rotation in the reflection coefficient angles is anticlockwise with increasing frequency. It is not possible to realize these reactance values accurately over the passband with a passive network. Avoiding the resonance regions is more realistic in wideband designs.

The reflection coefficient angles (θ_R) can be constrained to the regions shown below to avoid the resonance regions:

1.4 GHz: $118° > \theta_R > 245°$; 2.6 GHz: $188° > \theta_R > 282°$; 3.8 GHz: $237° > \theta_R > 338°$.

These regions correspond to more than 64% of the Smith chart circumference (1.4 GHz: 64%; 2.6 GHz: 73%; 3.8 GHz: 71%).

Note that the power is higher and the efficiency lower for reflection coefficient angles lower than the marked regions, while the reverse applies for higher reflection coefficient angles. Instead of targeting both regions, the upper region can be targeted for better efficiency, while the lower region can be targeted for higher power.

It was shown that the *H2DR* phase at a given frequency is almost constant away from the resonance region. To explore the sensitivity of this phase to the load network, the load matching network in Figure 5 was removed and the drain was terminated in a 50 Ω load. With this change, the efficiency decreased significantly, the minimum power dropped by 0.5 dBm, the small-signal gain decreased by 2.7 dB and the worst-case input VSWR changed to 1.5 from 1.15. The corresponding traces for Z_{Si_H2} and the *H2DR* are shown in Figure 9. Compared to Figure 5, the variation in Z_{Si_H2} is larger in Figure 9, but the tuning angle for the lowest intrinsic source resistance (270° phase for *H2DR*) is similar. The magnitude of *H2DR* is larger (Note the difference in the scale factors used), but the phase response seems to be similar. To allow for better comparison, the *H2DR* magnitude and phase and Q_{Si} are plotted versus the external reflection coefficient angle in Figure 10. Compared to Figure 6, the phase and the magnitude are different in the resonance region, but the phase in the constant region is similar (227° minimum versus 233°). The *H2DR* phase away from the resonance region seems to be tolerant to reasonable changes in the load network, but the magnitude changed a lot.

The conduction angles of the intrinsic output currents and the harmonic content in the output circuit are dependent on both the magnitude and phase of *H2DR*. It follows from the above that the load network must be in place before the second-harmonic input performance can be optimized. Source-pull contours (Smith chart edge or full chart) can be generated with the load network in place to define acceptable regions for the second harmonic source termination. If harmonic contours cannot be generated, the resonance regions in the intrinsic *Qs* or the *H2DR* phase can be avoided instead. With both networks in place, the performance of the amplifier stage can be fine-tuned or optimized.

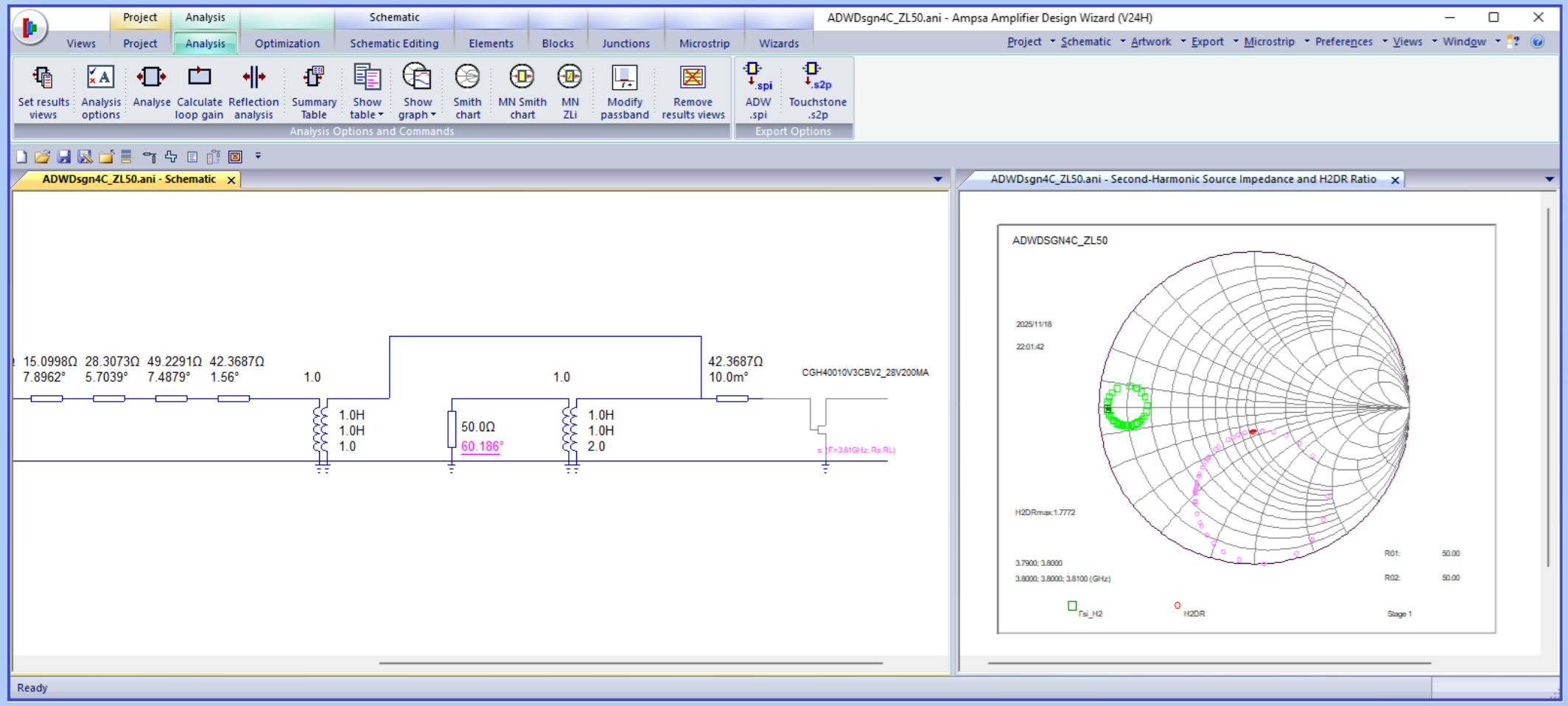

Figure 9. To illustrate the effect of the load network on the intrinsic input impedance, Z_{Si_H2} and *H2DR* are shown here with a 50 Ω load instead of the load matching network used in Figure 5.

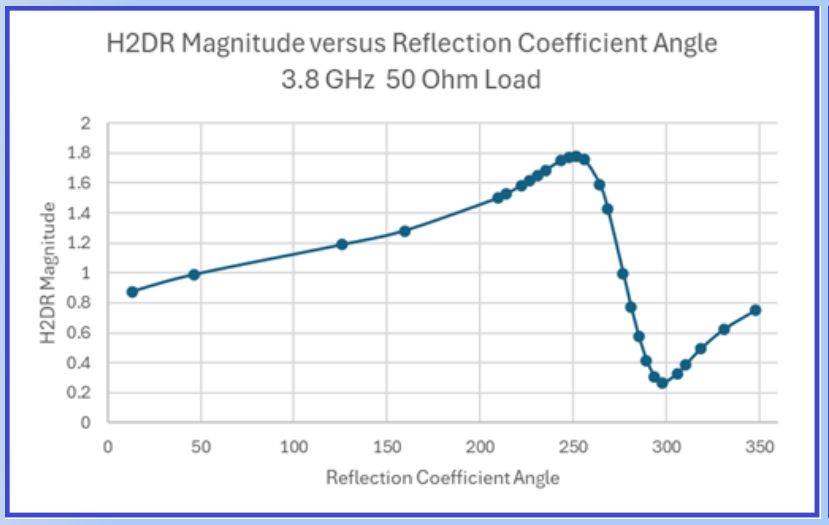

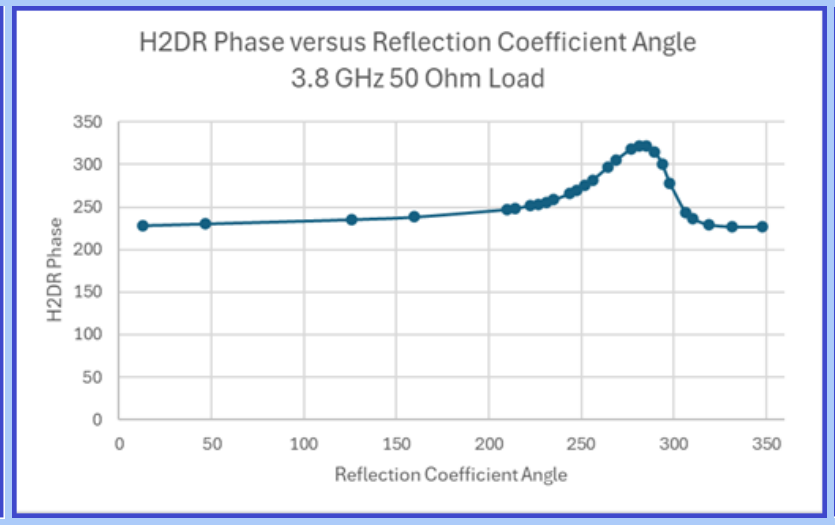

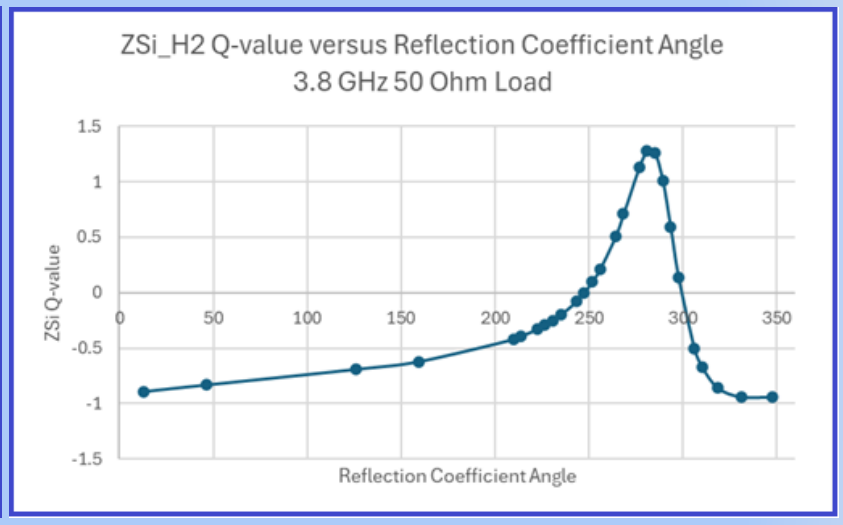

Figure 10. The *H2DR* magnitude and phase and the *Q*-value associated with Z_{Si} are plotted versus the reflection coefficient angle with load matching network in Figure 5 removed.

References

1. Tushar Sharma, Srinidhi E.R., Ramzi Darraji, Damon G. Holmes, Joseph Staudinger, Jeffrey K. Jones, and Fadhel M. Ghannouchi, “High-Efficiency Input and Output Harmonic Engineered Power Amplifiers”, IEEE Trans. Microwave Theory and Techniques, Vol. 66, No. 2, February 2018.

2. Sagar K. Dhar, Tushar Sharma, Ramzi Darraji, Damon G. Holmes, Suhas Veetil Illath, Vince Mallette and Fadhel M. Ghannouchi, IEEE Trans. Microwave Theory and Techniques, Vol. 67, No. 9, September 2019.

3. V. Tamrakar, S. Dhar , T. Sharma, and J. Mukherjee, "Investigation of input-output waveform engineered high-efficiency broadband class B/J power amplifier", IEEE Access, Vol. 10, 2022.

Thank you!

To learn more, visit www.ampsa.com

You can sign up for a trial or buy a license on Ampsa's website.